Martin Brodrecht, Bharti Kumari, Hergen Breitzke,
Torsten Gutmann and Gerd Buntkowsky*

Chemically Modified Silica Materials as Model Systems for the Characterization of Water-Surface Interactions

https://doi.org/10.1515/zpch-2017-1059
Received October 20, 2017; accepted December 7, 2017

Abstract: A series of novel functionalized mesoporous silica-based materials with well-defined pore diameters, surface functionalization and surface morphology is synthesized by co-condensation or grafting techniques and characterized by solid-state NMR spectroscopy, DNP enhanced solid state-NMR and thermodynamic techniques. These materials are employed as host-systems for small-guest molecules like water, small alcohols, carbonic acids, small aromatic molecules, binary mixtures and others. The phase-behavior of these confined guests is studied by combinations of one dimensional solid-state NMR techniques (^{1}H MAS, ^{2}H-line shape analysis, ^{13}C CPMAS) and two-dimensional correlation experiments like ^{1}H-^{29}Si- solid-state HETCOR.

Keywords: confinement; micro-phase separation; solid-state-NMR.

1 Introduction

In recent years, mesoscopically organized materials, which have characteristic structures on a length scale of 1 nm–100 nm, have developed into one of the most interesting research topics in the border area of physics, chemistry, biology and materials science. Due to their versatile properties such as thermal stability, large surface area, low specific weight, high surface functionality, tunable pore sizes and possible adaptation of the surface properties, they have a broad application

***Corresponding author: Gerd Buntkowsky,** Eduard-Zintl-Institute of Inorganic and Physical Chemistry, Technical University of Darmstadt, Alarich-Weiss-Str. 8, D-64287 Darmstadt, Germany, e-mail: gerd.buntkowsky@chemie.tu-darmstadt.de
Martin Brodrecht, Bharti Kumari, Hergen Breitzke and Torsten Gutmann: Eduard-Zintl-Institute of Inorganic and Physical Chemistry, Technical University of Darmstadt, Alarich-Weiss-Str. 8, D-64287 Darmstadt, Germany

spectrum, ranging over such diverse areas as catalysis, separation media, gas storage, transporters for medicaments, additives for polymers and more [1–5].

Typical representatives of these materials are mesoporous silica materials [6–18] (hereinafter referred to as silica materials). Their morphology is characterized e.g. by an ordered two-dimensional hexagonal array of cylindrical pores [Periodic Mesoporous Silica (PMS)] like the well-known MCM-41 [6] and SBA-15 [19, 20] materials, or by three-dimensional sponge-like structures as for example in the case of disordered glasses such as CPG-10-75 [21, 22] or Vycor.

The behavior of small fluid sample molecules (water, benzene, pyridine, isobutyric acid, naphthalene, biphenyl, ionic liquids, etc.) in the confinement of complex mesoporous systems is investigated by us for several years (see e.g. Werner et al. [23] and references therein). As hosts, pure and functionalized silica materials such as aminopropyltriethoxysilane (APTES) covered SBA-15 were used. Characterization was carried out using solid-state NMR spectroscopy at variable temperatures and diffusion measurements as well as thermodynamic methods such as Brunauer–Emmett–Teller (BET) analysis and differential scanning calorimetry (DSC). The structural and dynamic properties of these molecules were compared with the bulk properties in order to work out the influence of the confinement. Temperature-dependent ^{2}H NMR measurements provided information on dynamics in the systems, which are linked to phase transitions, which were also observed by DSC analyses. By means of ^{1}H solid-state NMR, the dynamics of water as well as the formation of hydrogen bonds were investigated more closely. For comparison carbon based mesoporous materials were investigated [24]. These studies have shown that the characterization of the guest molecules and their interaction with the host system by solid-state NMR methods is possible independently of the carrier material used (glass, silicate material, carbon).

Due to the presence of silanol (SiOH) groups on the pore walls, the surface properties (hydrophilic/hydrophobic, polar/non-polar, hydrogen-bond donors/acceptors) of these materials can be tailor-made with different chemical functions [4]. For this, covalent functional groups such as e.g. amino, amide, carboxyl, phosphate, chloride or peptide functions have to be introduced either by post-synthetic grafting or by co-condensation during the synthesis [3, 25, 26].

Owing to their versatility, PMS materials are ideally suited for fundamental studies of the effect of confinement on the structural, dynamic and thermophysical properties of fluids in general, and water in particular or protein solutions such as RNASE A [27]. This interest is motivated by the desire to better understand the influence of surface forces and finite-size effects on the behavior of the substrate in the pores [28]. Examples of such confinement effects include the change of the freezing and melting points or glass transitions of the confined liquids [28–32]. The main reason why PMS materials are so interesting models for

confinement effects is the complex interplay of interactions between the molecules themselves on the one hand and the molecules and the surface on the other hand. Since the pore diameter is typically a factor 10–100 greater than the size of the guest molecules, a substantial fraction of the guest molecules is in direct vicinity of the surface. As a result, the two types of interactions are of comparable magnitude. Moreover, both types of interactions might have the simple geometry dependence of an electrostatic or dispersion interaction or the complex angular behavior of a strong hydrogen bond.

The investigation of the phase-behavior in these confined systems depends strongly on both the pore diameter and the surface properties and can be studied by a number of techniques. The combination of solid-state NMR [23], thermodynamic techniques like differential scanning calorimetry (DSC) or thermogravimetric analysis (TGA) [33, 34] and computational techniques [35] is of high diagnostic value in the investigation of these systems (see e.g. [23, 27, 36–46]). In this combination NMR techniques provide insights at the molecular level into the structure of the materials themselves, into the dynamics of the guest molecules, and into the guest-host interactions at the interface.

However, solid-state NMR as a comparatively insensitive type of spectroscopy has currently still a major limitation since it relies on relatively large specific surfaces. Recently, the use of hyperpolarization methods such as dynamic nuclear polarization (DNP) has shown a solution to this sensitivity problem. In this method, the electron spin polarization of stable radicals, e.g. TEMPO or TOTAPOL is transferred into nuclear spin polarization by microwave irradiation. The paper by Griffin and co-workers [47] provides an overview of the application potential of DNP-amplified solid-state NMR spectroscopy. This method is very well suited for the investigation of surfaces of porous systems, as shown by Emsley and Lesage [48, 49]. It is of particular interest in this context that covalently attached radicals to silica surfaces allow a targeted local polarization of the adjacent ^{29}Si, ^{13}C, ^{15}N, etc. nuclei [50, 51].

In addition to these experimental studies, the theoretical modeling of the systems is of crucial importance for the understanding of the interactions. Of particular importance in this field are molecular dynamics calculations which correlate the effects of the geometric constraints and the surface properties with the dynamics and structure of the complex fluids, as demonstrated recently [52, 53].

Equally important for the interpretation of NMR data are quantum chemical calculations of NMR parameters such as the chemical shift. A decisive contribution was made by the development of the nuclear-independent chemical shifts (NICS) concept, which allows the calculation of surface-contribution to chemical shifts without the presence of specific probe molecules [54–56].

The main aim of the current paper is to give an overview how the controlled modification of the surfaces of mesoporous silica and the investigation of the influence of these modifications on the structure, dynamics and phase behavior of simple and binary fluids confined in the pores using methods of solid-state NMR spectroscopy leads to a better understanding of the confinement effects inside these pores.

The rest of this paper is organized as follows. First several examples of the surface modification of silica materials and their characterization by solid-state NMR are given. Then an overview about the behavior of small guest molecules inside their pores is given. Finally, some results on guest-molecules inside mesoporous carbon materials are reported.

2 Results and discussion

2.1 Water confined in modified silica pores

If the effects of confinement are to be studied it is important to investigate samples with high pore-surface/pore-volume ratio. Thus, samples with narrow pore diameters and very high surface homogeneity are needed. For this reason, SBA-15 type materials, which have rather large pore diameters [6] and comparably rough inner surfaces [36] are ill-suited, and special MCM-41 materials with narrow pore diameter (2.2 nm) functionalized by APTES were synthesized. For the characterization of these materials, ^{29}Si CP-MAS is employed. It allows a direct and fast monitoring of the surface silanol groups, the bulk silica atoms, and, if standard linkers like APTES are employed, also of the linker molecules attached to the surface. For pure silica materials there are four different binding types of surface silica sites, labeled by the number $\boldsymbol{n}$ of –O-Si ligands as Q_n-sites (Figure 1). In typical PMS materials only sites with n = 2–4 (Q_2, Q_3 or Q_4) are found. The silanol groups can serve as covalent anchoring points for an organic linker molecule. In the case of triethoxysilane linkers like APTES, the binding results in a new type of silica atoms called T_n-moieties (see Figure 1).

The lower panel of Figure 1 shows the ^{29}Si-CPMAS NMR spectra of neat silica and APTES functionalized silica. While in the neat silica only the Q_n-groups are present, the functionalized silica exhibits also the T_n-groups present at the surface of the silica material MCM-41. The presence of different T_n-groups confirms not only the successful surface modification but also characterizes the way of attachment of APTES to the silica surface.

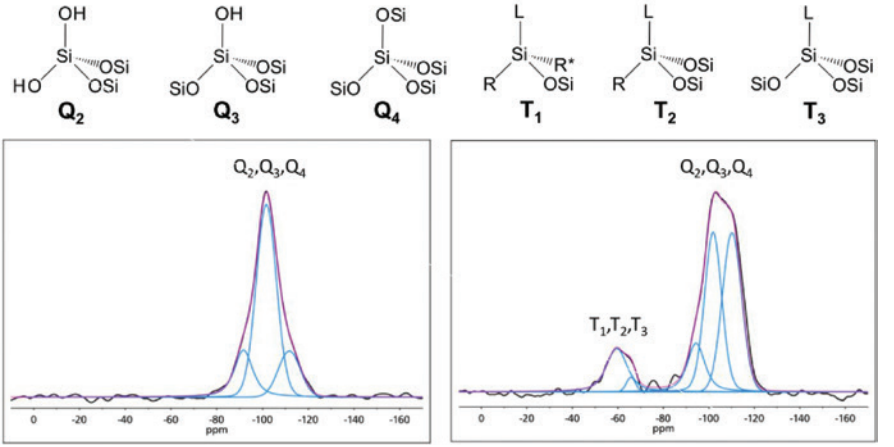

Fig. 1: Upper panel: The different types of silicon atoms in pure and functionalized silica materials are denoted as Q_n (n = 2–4), respectively T_n (n = 1–3). Lower panel: Typical ^{29}Si-CPMAS (10 kHz) spectra of neat silica (left) showing only Q_n-groups and of functionalized silica (right) showing both Q_n and T_n-groups. (Adapted from Weigler et al. [57]).

2.2 Surface modifications of PMS studied by solid-state NMR

Biological mineralization is one of the most interesting topics for material scientists [58, 59]. Nature manages the formation of hybrid materials made of an inorganic matrix and organic fibers to combine most desired and often reverse properties. In the case of mammal bones, it means a material made of hydroxylapatite and collagen which results in a combination of properties such as the robustness caused by apatite and flexibility caused by collagen. Another biomineralization process promoted by sillafins (polyamines) results in highly ordered siliceous inorganic support materials called diatoms [60–63]. Owing to their large application potential, silica based hybrid materials with various organic linkage are currently under intensive investigation [64]. A crucial step in understanding the molecular interface between the bioorganic molecule and the surface of the inorganic support material and their impact on e.g. dissolved molecules is the investigation of hybrid models, formed by the controlled binding of a biological molecule to an inorganic support surface [65], a strategy which is also at the heart of biological materials science and engineering [66, 67].

In the following an efficient functionalization approach of mesoporous silica materials and its structural characterization with solid state NMR is shortly described, see ref. [46] for details. As a tailored hybrid system, the collagen-like nonapeptide H-(Gly-Pro-Hyp)$_3$-OH was employed. It was grafted by a linker in a

controlled fashion to the inner surfaces of mesoporous silica as inorganic support material. Mesoporous silica was chosen instead of hydroxyapatite to enable the peptide to enter the pores thereby allowing better interfacial interactions and creating a new kind of hybrid material. The bound peptide was characterized by ^{13}C solid state NMR spectroscopy. For the proper identification of the binding sites, a combination of standard and DNP enhanced CP-MAS NMR for the detection of ^{15}N nuclei in natural abundance was utilized.

The upper panel of Figure 2 shows the ^{13}C CP-MAS spectra of ester activated silica material in combination with the nonapeptide. From (Figure 2a and b) it is evident that the peptide is indeed incorporated in the pores after immobilization. The covalent binding of the peptide is indicated by the decreased intensity of the characteristic peaks for the succinimidyl moiety at approx. 15 ppm when comparing

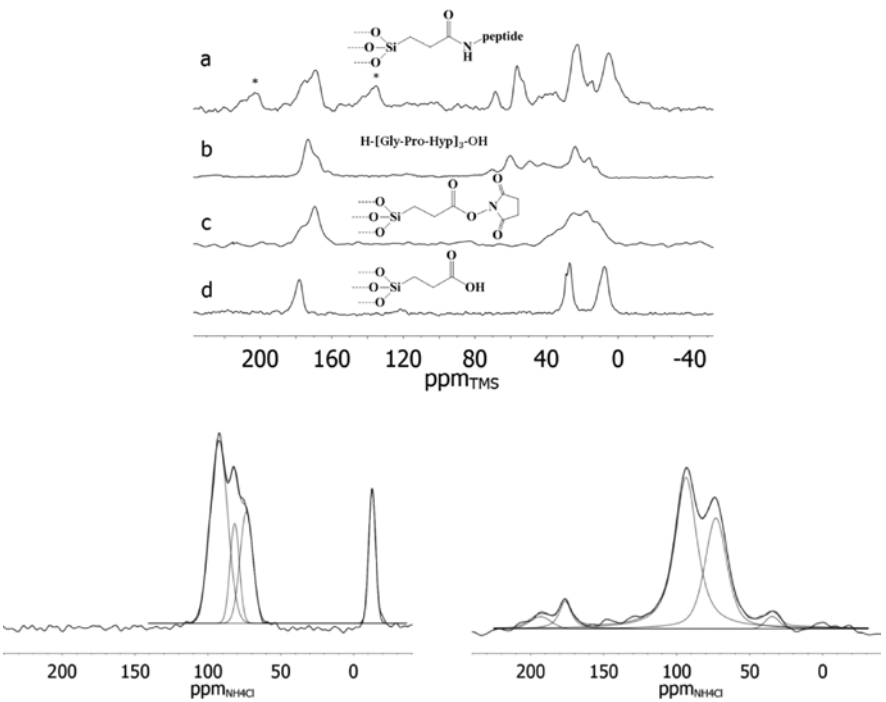

Fig. 2: Upper panel: Normalized 14 Tesla ^{13}C CP-MAS NMR (at 5 kHz) spectra of the immobilized (a) and the free (b) nonapeptide H-[Gly-Pro-Hyp]$_3$-OH; (c) the pre-activated silica TSTU-silica (at 10 kHz), and (d) the COOH- silica (at 10 kHz). Note: Signals marked with * refer to spinning sidebands. Lower panel: DNP enhanced ^{15}N CP-MAS NMR spectra and deconvolution of the (left) free nonapeptide H-[Gly-Pro-Hyp]$_3$-OH and the (right) immobilized H-[Gly-Pro-Hyp]$_3$-OH on TSTU-silica. (Adapted from ref. [46]).

the spectra of activated silica (Figure 2d) with the immobilization (Figure 2a). At the same time, the appearance of the characteristic peaks for the nonapeptide (Figure 2b) in the carbonyl as well as in the aliphatic region is observed. The latter indicates the exchange of the succinimidyl moiety with the nonapeptide.

For the decisive proof of the formation of an amide bond between the N-terminus of the peptide and the carboxyl-group of the linker ^{15}N-solid-state NMR spectra of the free and the immobilized peptide are mandatory. For favorable systems with high sensitivity, large amounts of sample material and narrow lines it is possible to detect natural abundance ^{15}N spectra of small peptides with standard CP-MAS NMR techniques [68]. For immobilized peptides, however, the situation is less fortunate. Since the absolute sensitivity of ^{15}N-solid state NMR is roughly a factor of 50 lower than of ^{13}C, to obtain a similar signal to noise ratio as in the ^{13}C spectrum (upper panel, 15.5 h measurement) a measurement time on the order of ca. 1600 days (4 years) would be necessary, which of course is not feasible. For this reason, the ^{15}N CP-MAS spectra had to be measured with DNP enhancement [69]. The lower panel compares the resulting DNP enhanced ^{15}N spectra before and after immobilization. In the left panel the N-terminus of the free peptide at –12 ppm is clearly visible. In the right panel this signal is no longer visible and new signals in the amide region (70–95 ppm) are visible, proving the formation of an amide bond between linker and peptide. Moreover, the broad ^{15}N-NMR signals of the amide signal indicate local structural disorder, most probably due to different hydrogen bonding situations, and a distribution of conformations. To the best of our knowledge, this was the first direct confirmation of a covalent bond of a peptide N-Terminus to TSTU-activated COOH-silica.

These measurements showed that it is feasible to immobilize collagen-like peptides on the surfaces of carboxylate functionalized SBA-15 and bio-active silica materials and to prove in detail the binding by a combination of ^{13}C-CPMAS and DNP enhanced ^{15}N-CPMAS solid state NMR spectroscopy without any costly or chemically unfeasible isotope labeling.

2.3 Surface modifications of SiO_2 coated polycarbonate membranes studied by DNP assisted solid-state NMR

While solid-state NMR is ideally suited for the characterization of mesoporous silica materials with their large inner surfaces, it generally fails if systems with lower surface areas are to be investigated, owing to the low sensitivity of NMR. In this situation hyperpolarization techniques and in particular DNP enhanced solid-state NMR [48] can help to make these systems amenable for solid-state NMR. Functionalized etched ion-track membranes based on polycarbonate (PC)

or polyethylene terephthalate (PET) are typical examples where this problem is grave. In a recent study we applied the DNP enhanced NMR technique [70] to investigate the functionalization of the inner-pore surfaces of porous etched ion-track membranes conformally coated with a 5 nm thin SiO_2 layer by atomic layer deposition (ALD) and subsequently modified by aminopropyl silane linkers.

The functionalization of these membranes is monitored by DNP enhanced ^{13}C- and ^{29}Si-solid state NMR. As an example, Figure 3b shows the ^{29}Si solution NMR spectrum of neat APTES (lower trace) and the ^{29}Si DNP enhanced spectrum of the APTES functionalized membrane (center trace and enlarged as top trace). The signals of the T_n-groups are clearly visible in the DNP enhanced spectrum, showing the successful functionalization of the silica coated ion-tracks. For further details see the paper by Kumari et al. [70].

2.4 Water confined in silica

Water molecules with their high polarity and their ability to form hydrogen bonded network among themselves and with suitable hydrogen donors and acceptors are the primary solvent for most naturally occurring chemical and biological reactions. On surfaces there is a competition between the surface-liquid and liquid-liquid hydrophobic, hydrophilic hydrogen bond interactions. As the result of this competition in general two different types of water are observed namely bound water near the pore surface, which often form glass-like structures ("non-freezable water") and free water molecules with a behavior similar to bulk water. Silica materials have a very strong affinity towards water. Owing to this strong hygroscopic behavior they are technically employed as drying material.

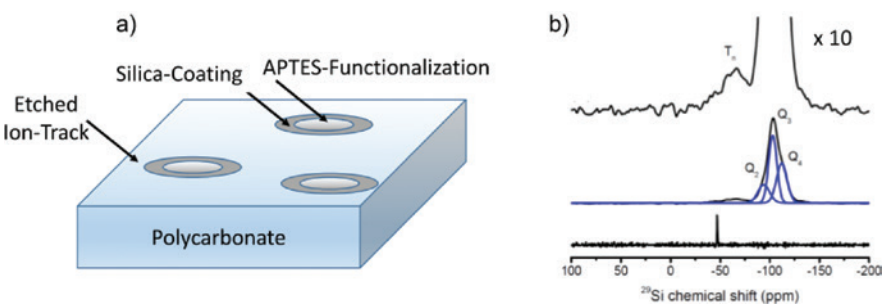

Fig. 3: (a) Sketch of the polycarbonate-membrane with silica coated etched ion-tracks, functionalized by linker groups like APTES. (b) By DNP enhancement it is feasible to reveal e.g. the APTES functionalization in ^{29}Si-CP-MAS spectra via the occurrence of the T_n-groups, which are not visible without DNP enhancement (after [70]).

Several years ago some of us studied the adsorption behavior of water inside mesoporous MCM-41, SBA-15 [37] and the controlled porous glass CPG-10-75 [41] employing ^{1}H-solid state NMR. In these systems we found that initially a monomolecular layer of water molecules is adsorbed on the silica surface, whose area grows until all surface-silanol groups are saturated by hydrogen bonding. Moreover, upon increasing the water content it was found that for small pore diameters (3.3 nm, MCM-41) pore-condensation causes a bimodal distribution of water environments while for larger pore diameters (8 nm SBA-15, 10.3 nm CPG-10-75) a continuous growth of the water layers from the silica wall towards the pore center is observed.

These previous results prompted us to investigate the processes of drying and refilling mesoporous silica materials in more detail [71] employing a combination of magic-angle spinning (MAS) solid-state NMR, dielectric spectroscopy (BDS) and calorimetric measurements. In the NMR spectra a coexistence of several different water species were found, which are characterized by their chemical shifts according to Grünberg et al. [37] By drying the samples inside the MAS rotor it was found that a very good vacuum ($\approx 10^{-6}$ mbar) is necessary to remove all H_2O molecules from the silica matrices.

Time-dependent ^{1}H-NMR-spectra recorded after loading the samples (see Figure 4) indicate a very specific course of water, first existing in a bulk-like form inside the pores and then distributing itself through the pores by hydrogen bonding to surface silanol groups. After assuring accurate sample loading by those means, it was possible to investigate lowly hydrated samples of water

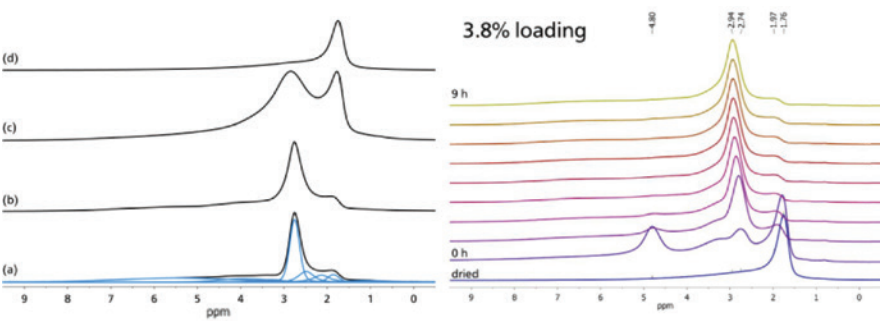

Fig. 4: Room temperature ^{1}H MAS-NMR spectra of an MCM-41 sample at 10 kHz (adapted from ref. [71]): Left panel: (a): Untreated sample (b): Sample dried at 180 °C (453.15 K) under atmospheric pressure for 24 h. (c): Sample dried at room temperature under mild vacuum (10^{-1} mbar, 24 h).(d): Sample dried at room temperature under high vacuum (10^{-6} mbar, 24 h). -All spectra are normalized to equal height. Right panel: Sample filled with 0.7% (left) of water referred to the pore volume. Spectra measured at time intervals of 1 h. Bottom: the dry sample.

confined in MCM-41 via DSC and BDS at temperatures below the bulk-water freezing point and find two non-crystallizing water species with Arrhenius behavior and activation energies of 0.53 eV (see [71] for details). Moreover spin-lattice relaxation measurements and stimulated echo experiments by the Vogel group revealed the temperature dependent dynamics of water inside the confinement [45].

2.5 Water confined in modified silica pores

The APTES modified silica materials described above were employed in ^{2}H-solid state NMR and BDS to reveal the dynamics of water inside these modified silica materials. ^{2}H spin-lattice relaxation measurements revealed that below ca. 210 K the liquid water species becomes accompanied by a solid water species, causing an onset of a bimodal relaxation curve. Moreover, the reorientation of the liquid water species is governed by a pronounced dynamical heterogeneity in the investigated temperature range. The variations in the temperature dependence are attributed to a change from bulk-like behavior towards interface-dominated dynamics (see Weigler et al. [57] for further details on the experimental results and their interpretation).

2.6 Naphthalene or biphenyl confined in silica

In previous studies on the behavior of benzene in mesoporous silica [29, 38], it was found that the rather weak interactions of the aromatic ring with the pore surfaces lead to a very interesting dynamic behavior. A similar phase behavior is also expected for the next bigger bicyclic aromatic compounds (biphenyl and naphthalene). The essential difference between the two systems is that biphenyl has an internal degree of rotational freedom (twisting of the two phenyl rings), whereas naphthalene is a rigid aromatic without internal degrees of freedom of rotation. The host material used in the case of biphenyl silylated and non-silylated was MCM-41 with pore diameters of 2.5 nm and 2.9 nm, respectively. In the case of the naphthalene, an MCM-41 material with 3.3 nm pore diameter was used.

2.6.1 Biphenyl

In the case of biphenyl (Figure 5) the typical ^{2}H-Pake pattern of a rigid aromatic -CD group is observed at low temperatures (Q_{zz} = 132 kHz, corresponding to a

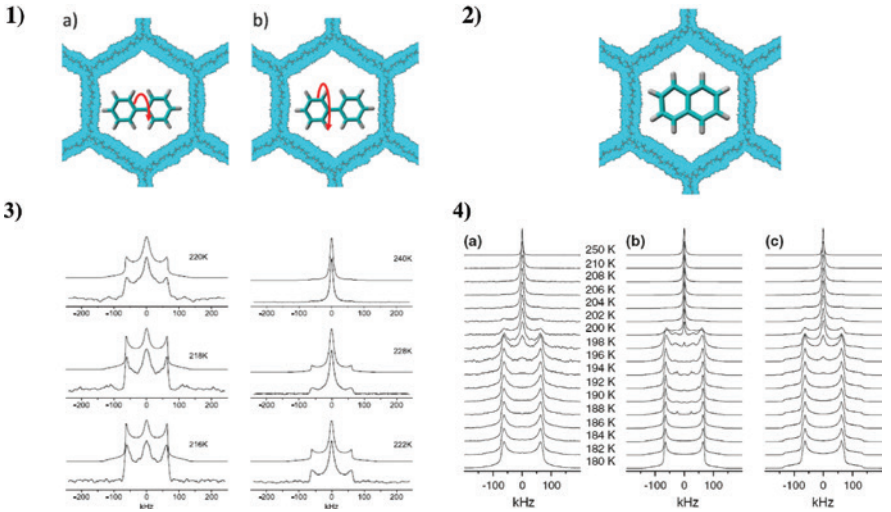

Fig. 5: Upper panel: Schematic representation of the guest molecules **1** biphenyl [43] und **2** naphthalene [72] inside mesoporous silica. The red arrows in 1a) and 1b) mark the possible rotations, which can explain the observed spectra. 3): experimental (lower trace) and simulated (upper trace) ^{2}H NMR spectra of biphenyl-d_{10} in silylated MCM-41 (2.9 nm pore diameter) as a function of temperature (according to de-Sousa-Amadeu et al. [43]) 4): experimental (a) and simulated (b, c) ^{2}H-NMR spectra of the melting process of naphthalene-d_8 in MCM-41 (3.3 nm pore diameter). Simulation (c) describes the transition from the rigid to the fluid phase with a two-phase model into a disordered glassy system. The simulation in (b) is based on an octahedral step model with a defined activation energy (adapted from Grünberg et al. [73]).

quadrupole coupling constant of $Q_{cc} = 176$ kHz and an asymmetry parameter of $\eta = 0.04$). Upon increasing the temperature, the spectra transform into the typical Lorentzian liquid spectra after exhibiting an intermediate range. The behavior of the biphenyl molecules in the transition region can be described well by a thermally activated process with a broad distribution of correlation times (Figure 6, left), and the distribution of activation energies for the individual samples under the assumption of the two-phase model of Roessler et al. [74] (Figure 6, right). This behavior is characteristic of a glass-like, highly disordered amorphous phase, similar to the situation of benzene in mesoporous silica. The ^{2}H NMR spectra shortly below the transition temperature exhibit interesting deviations from the simple Pake form, which are an indication of an onset of non-isotropic motions of the biphenyl molecules, such as e.g. C_2 flips of the phenyl rings, which precede the actual melting process. In all samples, a strong reduction of the melting point compared to the bulk (342.6 K) was observed by more than 100 K

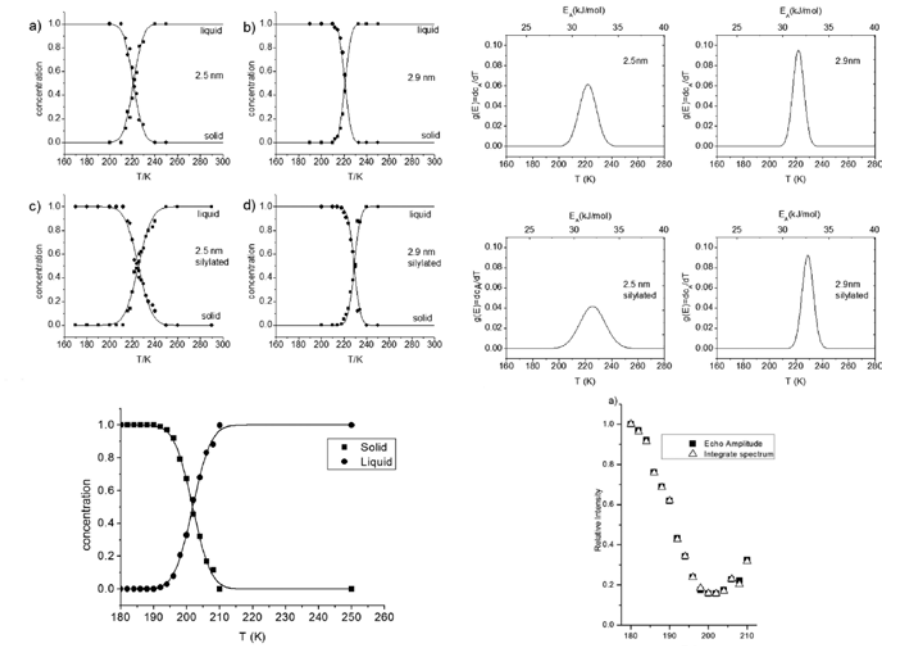

Fig. 6: Upper panel: analysis of the phase behavior of biphenyl in MCM-41. Left: relative proportions of the liquid and solid biphenyl molecules and right: the corresponding distribution of activation energies (adapted from de-Sousa-Amadeu et al. [43]). Lower panel: analysis of the phase behavior of biphenyl in MCM-41. Both the narrow phase-transition range and the strong reduction of the ^{2}H-echo NMR amplitude are indicative for a plastic crystalline phase (adapted from Grünberg et al. [73]).

down to 222 K–229 K. The final value of the melting point depends on both the pore diameter and the surface preparation.

2.6.2 Naphthalene

In the previous investigations of naphthalene confined in silica a strong reduction of the melting point in the pores of the naphthalene (^{1}H-MAS and ^{2}H-NMR) was observed. In order to analyze the underlying processes more precisely, a detailed analysis of the ^{2}H-solid-echo NMR spectra as a function of the temperature was carried out (Figure 5).

The temperature dependence looks very similar to the biphenyl with the typical ^{2}H-Pake spectrum at low temperatures, a liquid-like high-temperature spectrum and characteristic intermediate spectra. Again, a strong reduction of

the melting point by 152 K is observed. In contrast to biphenyl, these spectra show no signs of a premelting process. Moreover, in contrast to biphenyl, the changes in the shape of the lines and the echo-amplitude (see Figure 6) can be equally well described both with the Roessler model [74], with a narrow glassy distribution of activation energies, as well as with a more crystalline model with narrow distribution. This is an indication of a plastically crystalline phase within the pores. Such a phase has also been proposed for naphthalene in ball-milled silica [75–78]. This proposal was later supported by DSC, Raman spectroscopy, and powder diffractometry on naphthalene in mesoporous silica [72].

2.7 Phase behavior of the binary system water and isobutyric acid confined in silica

Mixtures of water and isobutyric acid (iBA, 2-methylpropanoic acid) are ideal models for the investigation of binary fluids inside confinement, owing to their favorable phase diagram. iBA, a carboxylic acid, has both hydrophilic and hydrophobic functional groups, leading to phase separation when mixed with water.

A long standing problem is the question of the micro-phase separation of water-isobutyric acid mixtures confined inside mesoporous silica hosts. Part of this problem was solved several years ago by some of us, employing a combination of ^{1}H-NMR relaxometry and diffusometry [39, 41, 42] to investigate binary mixtures of water with iBA confined in mesoporous silica materials. In these experiments an anomalous temperature dependence of the self-diffusion coefficient and a bifurcation of the T_2-relaxation upon a critical temperature of 42 °C was observed, indicating concentric layers as the phase-structure below the critical temperature. Since at that time it was not possible to determine to which phase (inner or outer) the different proton-chemical shifts belong, these findings were then interpreted tentatively as the results of a phase-separation between a water rich phase close to the pore walls and an iBA rich phase in the center of the pores below the critical temperature. Owing to recent advances in low-temperature experimental methodology (low-temperature MAS HETCOR) and molecular dynamics simulations we decided to revisit this system to solve this open question [79].

Since the phase-separated state is the thermodynamically stable state in the bulk-mixture, we assumed that, if a phase-separated state is present in the pores at room temperature, it will be stable upon decrease of the temperature and thus observable at low temperatures. There, the molecular motions are frozen and details of the dipolar interactions between the surface and the iBA protons are visible. By two-dimensional ^{29}Si/^{1}H-FSLGHETCOR experiments it is possible to monitor the resolved magnetic dipolar interactions between protons and the

silica nuclei on the surface. From this information it is feasible to decide, which molecules are closer to the surface. Accordingly, we performed low-temperature $^{1}H/^{29}Si$-FSLGHETCOR experiments on an iBA/H_2O mixture inside in SBA-15. As a typical example, Figure 7 displays the resulting spectra for contact times of 3 ms and 0.5 ms. All types of protons exhibit a cross peak with the ^{29}Si-signal. In the ^{1}H-dimension the strong signal at ca. 6.5 ppm assigns to hydroxyl groups from H_2O molecules, which are in fast exchange with the carboxyl-protons of COOH in iBA and the silanol-protons [37] of the silica. This chemical shift is in agreement with an assumed iBA enriched phase. The second strong signal at 1.2 ppm is assigned to aliphatic protons of the iBA. In addition, there is a weak signal at 11.5 ppm, which assigns to non-exchanging protons from the carboxyl group of the iBA. For details see [79]. In the spectrum with the shorter contact time only the short distances are strongly visible (see right panel of Figure 7). From this spectrum it is evident that the hydroxyl-protons are mainly correlated to the Q_2 and Q_3 groups and the main correlation of the aliphatic protons is with the Q_4 groups (note that the ratio of Q_n groups is non-stoichiometric, since only groups near protons are visible). From the combination of these experimental data and the MD-simulations performed by the Drossel group, it was possible to finally solve the long-standing problem of the micro-phase separation inside these materials and show that the iBA rich phase is close to the pore-wall and the water-rich phase is in the center of the pores, in contrast to previous assumptions. The MD simulations reveal that this surprising phase-behavior is mainly the result of the minimization of the hydrogen-bonding enthalpy. Moreover, the simulations

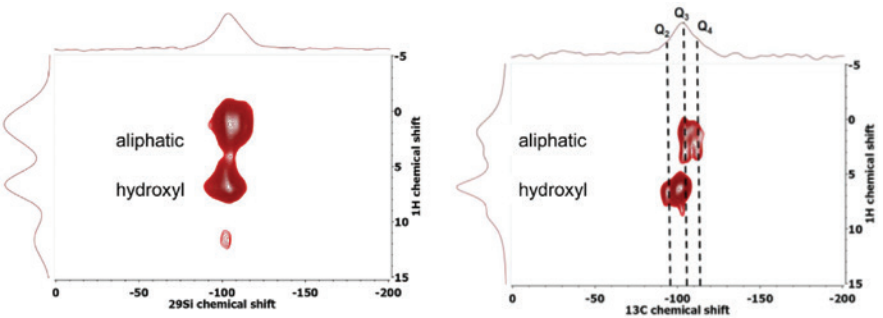

Fig. 7: Low temperature 9.4 Tesla $^{1}H/^{29}Si$-FSLGHETCOR experiments of iBA/H_2O mixtures of 56 wt% iBA inside mesoporous SBA-15, measured at nominally 100 K and with a rotation frequency of 8 kHz. During the evolution time FSLG homonuclear decoupling [80] was applied with a decoupling field of 89 kHz to reveal the ^{1}H-chemical shifts in the indirect dimension. Left panel: 3 ms contact time; right panel: at 0.5 ms contact time (adapted from ref. [79]).

showed also that upon increasing temperature the relative water concentration increases at the pore surface, which is attributed to entropic contributions, which lead to a more thorough miscibility.

2.8 Phase behavior of binary system water and alcohol confined in silica

Preliminary unpublished results show that also pure alcohol and binary water/alcohol mixtures confined in mesoporous silica can be investigated by the same ^{1}H-^{29}Si-HETCOR experiments (see Figure 8). By varying the contact time in the HETCOR-experiment it was possible for neat 1-octanol to map out the correlations between hydroxyl-protons and silica-surface (3 ms) and additionally also at 9 ms the correlations between aliphatic protons and silica-surface.

2.9 Guest molecules confined in mesoporous carbon materials

In addition to silica as host, we also performed some studies of benzene, water, and pyridine confined in mesoporous carbon or silica templated carbon materials [24]. By solid-state NMR it was possible to reveal on the active groups on the carbon-surface as a function of the carbonization temperature employed in the preparation of the samples (see Figure 9). By means of the chemical shift (CS) changes during absorption of the guest molecules on the surface it was possible

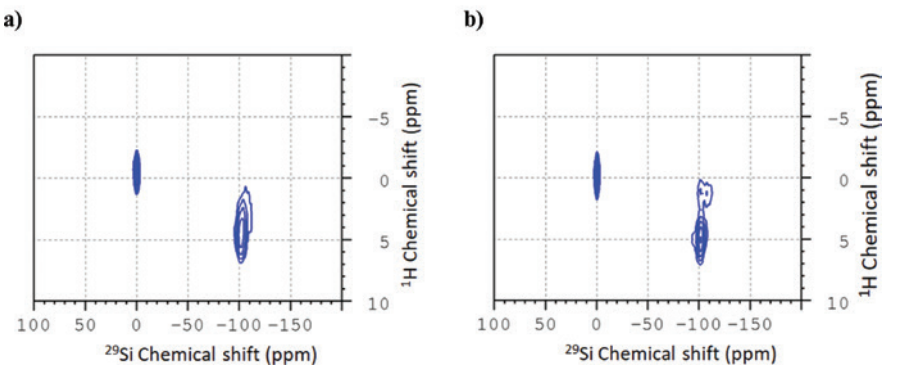

Fig. 8: Room temperature ^{1}H-^{29}Si FSLGHETCOR experiment measured at 8 kHz spinning. (a) Dried SBA-15 mixed with neat octanol-1 measured with a contact time of 3 ms. (b) Dried SBA-15 mixed with neat octanol-1 measured with a contact time of 9 ms (unpublished results).

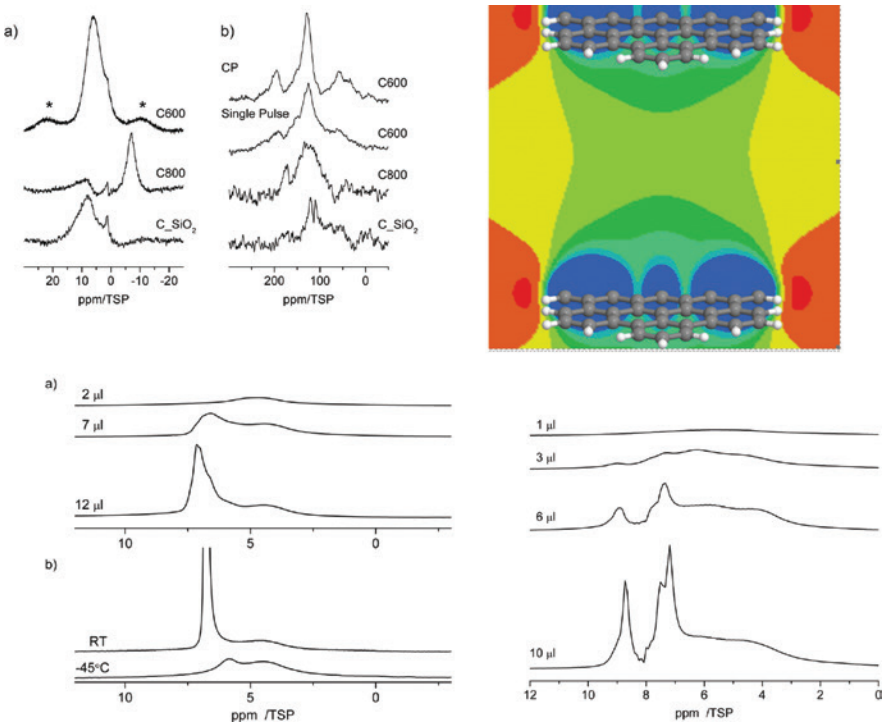

Fig. 9: Upper panel: Left: ^{1}H and ^{13}C-MAS NMR spectra of mesoporous carbon materials carbonized at 600 °C and 800 °C and silica templated carbon. Note: signals marked with asterisks are spinning sidebands. Right: calculated chemical shift changes inside carbon employing hexabenzocorone stacks as model. The green and blue areas correspond to shift changes between –2 and –6 ppm. Lower panel: Left a) ^{1}H MAS NMR of benzene inside C600 at RT. Right: ^{1}H NMR spectra recorded at 10 kHz spinning speed of pyridine in C600 for different loadings between 1 mL and 10 mL (adapted from Xu et al. [24]).

to monitor the absorbed species. For the interpretation of these CS changes, NICS calculations were performed by the collaborating Sebastiani group.

3 Conclusion

This review paper presents some recent advances on the synthesis of well-defined mesoporous host materials and the characterization of small molecules confined in these materials employing in particular solid-state NMR techniques. Several exemplary studies of confined polar molecules such as water, alcohols, carbonic acids or binary mixtures of these compounds as well as unpolar aromatic

molecules including naphthalene and biphenyl inside mainly silica based host systems with different surface properties are described.

It turns out that solid state NMR is not only one of the most versatile techniques for the monitoring of the surface functionalization of the hosts but also an ideal tool for differentiating between bound, adsorbed and free molecules inside the pores. Next to the standard cross polarization experiments such as ^{29}Si or ^{13}C CP MAS which enable to distinguish the binding sites of the linker to the surface, more complex techniques including in particular two dimensional HETCOR techniques shed more light on the structural arrangement of the constituents of binary systems inside the confinement. These structural studies are strongly supported by DNP techniques, which permit e.g. the detection of nitrogen containing functional groups on the surface in natural abundance without isotope enrichment. Variable temperature dependent ^{2}H solid state NMR allows the detection of rotational dynamics of organic molecules adsorbed in porous materials and helps to analyze unusual phase transitions in confinement.

Acknowledgements: Financial support by the Deutsche Forschungsgemeinschaft DFG in the frame-work of the special research unit FOR 1583 under contract Bu-911-18-1/2 is gratefully acknowledged.

References

1. M. S. Morey, A. Davidson, G. D. Stucky, J. Porous Mat. **5** (1998) 195.
2. H. T. Chen, S. Huh, J. W. Wiench, M. Pruski, V. S. Y. Lin, J. Am. Chem. Soc. **127** (2005) 13305.
3. X. G. Wang, K. S. K. Lin, J. C. C. Chan, S. F. Cheng, J. Phys. Chem. B **109** (2005) 1763.
4. A. Vinu, K. Z. Hossain, K. Ariga, J. Nanosci. Nanotec. **5** (2005) 347.
5. A. Vinu, M. Miyahara, K. Ariga, J. Nanosci. Nanotec. **6** (2006) 1510.
6. J. S. Beck, J. C. Vartuli, W. J. Roth, M. E. Leonowicz, C. T. Kresge, K. D. Schmitt, C. T. W. Chu, D. H. Olson, E. W. Sheppard, S. B. Mccullen, J. B. Higgins, J. L. Schlenker, J. Am. Chem. Soc. **114** (1992) 10834.
7. A. Sayari, S. Hamoudi, Chem. Mater. **13** (2001) 3151.
8. M. Vallet-Regi, A. Ramila, R. Del Real, J. Pérez-Pariente, Chem. Mater. **13** (2001) 308.
9. P. Selvam, S. K. Bhatia, C. G. Sonwane, Ind. Eng. Chem. Res. **40** (2001) 3237.
10. A. Schreiber, I. Ketelsen, G. H. Findenegg, Phys. Chem. Chem. Phys. **3** (2001) 1185.
11. F. Schüth, W. Schmidt, Adv. Eng. Mat. **4** (2002) 269.
12. S. R. Hall, D. Walsh, D. Green, R. Oreffo, S. Mann, J. Mater. Chem. **13** (2003) 186.
13. T. Linssen, K. Cassiers, P. Cool, E. Vansant, Adv. Colloid Interface Sci. **103** (2003) 121.
14. A. Adamczyk, Y. Xu, B. Walaszek, F. Roelofs, T. Pery, K. Pelzer, K. Philippot, B. Chaudret, H.-H. Limbach, H. Breitzke, Top. Catal. **48** (2008) 75.
15. R. Mellaerts, J. A. G. Jammaer, M. Van Speybroeck, H. Chen, J. Van Humbeeck, P. Augustijns, G. Van den Mooter, J. A. Martens, Langmuir **24** (2008) 8651.
16. T. Ukmar, T. Cendak, M. Mazaj, V. Kaucic, G. Mali, J. Phys. Chem. C **116** (2012) 2662.

17. A. Grünberg, H. Breitzke, G. Buntkowsky, Solid State NMR of Immobilized Catalysts and Nanocatalysts, In *Spectroscopic Properties of Inorganic and Organometallic Compounds: Techniques, Materials and Applications*, J. Yarwood, R. Douthwaite, S. Duckett, Eds. Royal Society of Chemistry, Cambridge, UK (2012), P. 289.
18. T. Gutmann, A. Grünberg, N. Rothermel, M. Werner, M. Srour, S. Abdulhussain, S. Tan, Y. Xu, H. Breitzke, G. Buntkowsky, Solid State Nucl. Mag. **55–56** (2013) 1.
19. D. Y. Zhao, J. L. Feng, Q. S. Huo, N. Melosh, G. H. Fredrickson, B. F. Chmelka, G. D. Stucky, Science **279** (1998) 548.
20. D. Y. Zhao, Q. S. Huo, J. L. Feng, B. F. Chmelka, G. D. Stucky, J. Am. Chem. Soc. **120** (1998) 60246.
21. L. D. Gelb, K. E. Gubbins, R. Radhakrishnan, M. Sliwinska-Bartkowiak, Rep. Prog. Phys. **62** (1999) 1573.
22. U. Ciesla, F. Schüth, Microporous Mesoporous Mater. **27** (1999) 131.
23. M. Werner, N. Rothermel, H. Breitzke, T. Gutmann, G. Buntkowsky, Isr. J. Chem. **54** (2014) 60.
24. Y. P. Xu, T. Watermann, H. H. Limbach, T. Gutmann, D. Sebastiani, G. Buntkowsky, Phys. Chem. Chem. Phys. **16** (2014) 9327.
25. A. S. Maria Chong, X. S. Zhao, J. Phys. Chem. B **107** (2003) 12650.
26. T. Yokoi, H. Yoshitake, T. Tatsumi, J. Mater. Chem. **14** (2004) 951.
27. M. Kahse, M. Werner, S. Zhao, M. Hartmann, G. Buntkowsky, R. Winter, J. Phys. Chem. C **118** (2014) 21523.
28. C. Alba-Simionesco, B. Coasne, G. Dosseh, G. Dudziak, K. Gubbins, R. Radhakrishnan, M. Sliwinska-Bartkowiak, J. Phys. Condens. Mat. **18** (2006) 15.
29. E. Gedat, A. Schreiber, J. Albrecht, I. Shenderovich, G. Findenegg, H.-H. Limbach, G. Buntkowsky, J. Phys. Chem. B **106** (2002) 1977.
30. P. Medick, T. Blochowicz, M. Vogel, E. Roessler, J. Non-Cryst. Solids **307** (2002) 565.
31. G. Dosseh, Y. Xia, C. Alba-Simionesco, J. Phys. Chem. **107** (2003) 6445.
32. S. A. Lusceac, C. Koplin, P. Medick, M. Vogel, N. Brodie-Linder, C. LeQuellec, C. Alba-Simionesco, E. A. Roessler, J. Phys. Chem. B **108** (2004) 16601.
33. G. Höhne, W. F. Hemminger, H.-J. Flammersheim, Differential Scanning Calorimetry, Springer, Berlin Heidelberg (2003).
34. W. F. Hemminger, H. K. Cammenga, Methoden der thermischen Analyse, Springer Berlin (1989).
35. M. Schoen, S. H. L. Klapp, Nanoconfined Fluids. Soft Matter Between Two and Three Dimensions Volume 24, John Wiley & Sons, New York (2007).
36. I. Shenderovich, G. Buntkowsky, A. Schreiber, E. Gedat, S. Sharif, J. Albrecht, N. S. Golubev, G. H. Findenegg, H. H. Limbach, J. Phys. Chem. B **107** (2003) 11924.
37. B. Grünberg, T. Emmler, E. Gedat, I. Shenderovich, G. H. Findenegg, H. H. Limbach, G. Buntkowsky, Chem.-Eur. J. **10** (2004) 5689.
38. W. Masierak, T. Emmler, E. Gedat, A. Schreiber, G. H. Findenegg, G. Buntkowsky, J. Phys. Chem. B **108** (2004) 18890.
39. A. Vyalikh, T. Emmler, E. Gedat, I. Shenderovich, G. H. Findenegg, H.-H. Limbach, G. Buntkowsky, Solid State NMR **28** (2005) 117.
40. G. Buntkowsky, H. Breitzke, A. Adamczyk, F. Roelofs, T. Emmler, E. Gedat, B. Grünberg, Y. Xu, H. H. Limbach, I. Shenderovich, A. Vyalikh, G. H. Findenegg, Phys. Chem. Chem. Phys. **9** (2007) 4843.
41. A. Vyalikh, T. Emmler, B. Grünberg, Y. Xu, I. Shenderovich, G. H. Findenegg, H.-H. Limbach, G. Buntkowsky, Z. für Phys. Chem. **221** (2007) 155.

42. A. Vyalikh, T. Emmler, I. Shenderovich, Y. Zeng, G. H. Findenegg, G. Buntkowsky, Phys. Chem. Chem. Phys. **9** (2007) 2249.
43. N. de-Sousa-Amadeu, B. Grünberg, J. Frydel, M. Werner, H.-H. Limbach, H. Breitzke, G. Buntkowsky, Z. Phys. Chem. **226** (2012) 1169.
44. S. Jayanthi, M. Werner, Y. Xu, G. Buntkowsky, S. Vega, J. Phys. Chem. C **117** (2013) 13114.
45. M. Sattig, S. Reutter, F. Fujara, M. Werner, G. Buntkowsky, M. Vogel, Phys. Chem. Chem. Phys. **16** (2014) 19229.
46. M. Werner, A. Heil, N. Rothermel, H. Breitzke, P. B. Groszewicz, A. S. Thankamony, T. Gutmann, G. Buntkowsky, Solid State Nucl. Mag. **72** (2015) 73.
47. A. Barnes, G. De Paepe, P. Van der Wel, K.-N. Hu, C.-G. Joo, V. Bajaj, M. Mak-Jurkauskas, J. Sirigiri, J. Herzfeld, R. Temkin, R. G. Griffin, App. Magn. Res. **34** (2008) 237.
48. A. Lesage, M. Lelli, D. Gajan, M. A. Caporini, V. Vitzthum, P. Mieville, J. Alauzun, A. Roussey, C. Thieuleux, A. Mehdi, G. Bodenhausen, C. Coperet, L. Emsley, J. Am. Chem. Soc. **132** (2010) 15459.
49. M. Lelli, D. Gajan, A. Lesage, M. A. Caporini, V. Vitzthum, P. Mieville, F. Heroguel, F. Rascon, A. Roussey, C. Thieuleux, M. Boualleg, L. Veyre, G. Bodenhausen, C. Coperet, L. Emsley, J. Am. Chem. Soc. **133** (2011) 2104.
50. D. Gajan, M. Schwarzwälder, M. P. Conley, W. R. Grüning, A. J. Rossini, A. Zagdoun, M. Lelli, M. Yulikov, G. Jeschke, C. Sauvée, O. Ouari, P. Tordo, L. Veyre, A. Lesage, C. Thieuleux, L. Emsley, C. Copéret, J. Am. Chem. Soc. **135** (2013) 15459.
51. A. S. L. Thankamony, O. Lafon, X. Lu, F. Aussenac, M. Rosay, J. Trebosc, H. Vezin, J.-P. Amoureux, App. Magn. Res. **43** (2012) 237.
52. M. F. Harrach, B. Drossel, J. Chem. Phys. **140** (2014) 174501.
53. E. Ackermann, E. M. Weiel, T. Pfaff, B. Drossel, Eur. Phys. J. E **35** (2012) 1.
54. P. v. R. Schleyer, C. Maerker, A. Dransfeld, H. Jiao, N. J. v. E. Hommes, J. Am. Chem. Soc. **118** (1996) 6317.
55. D. Sebastiani, ChemPhysChem **7** (2006) 164.
56. D. Sebastiani, K. N. Kudin, ACS Nano **2** (2008) 661.
57. M. Weigler, M. Brodrecht, H. Breitzke, F. Dietrich, M. Sattig, G. Buntkowsky, M. Vogel, Z. Phys. Chem. **232** (2018) 1041.
58. S. Mann, Biomineralization: Principles and Concepts in Bioinorganic Materials Chemistry Volume 5, Oxford University Press on Demand, Oxford (2001).
59. M. J. Duer, J. Magn. Reson. **253** (2015) 98.
60. M. Sumper, E. Brunner, Chembiochem **9** (2008) 1187.
61. N. Poulsen, M. Sumper, N. Kröger, Proc. Natl. Acad. Sci. USA **100** (2003) 12075.
62. E. Brunner, C. Groger, K. Lutz, P. Richthammer, K. Spinde, M. Sumper, Appl. Microbiol. Biotechnol. **84** (2009) 607.
63. N. Almqvist, Y. Delamo, B. L. Smith, N. H. Thomson, A. Bartholdson, R. Lal, M. Brzezinski, P. K. Hansma, J. Microsc. **202** (2001) 518.
64. N. Nassif, J. Livage, Chem. Soc. Rev. **40** (2011) 849.
65. Z. Zhou, F. Piepenbreier, V. R. R. Marthala, K. Karbacher, M. Hartmann, Catal. Today **243** (2014) 173.
66. M. Hartmann, X. Kostrov, Chem. Soc. Rev. **42** (2013) 6277.
67. I. Matlahov, Y. Geiger, G. Goobes, Phys. Chem. Chem. Phys. **16** (2014) 9031.
68. S. Jayanthi, B. Chatterjee, S. Raghothama, Biopolymers **91** (2009) 851.
69. A. Zagdoun, G. Casano, O. Ouari, G. Lapadula, A. J. Rossini, M. Lelli, M. Baffert, D. Gajan, L. Veyre, W. E. Maas, M. Rosay, R. T. Weber, C. Thieuleux, C. Coperet, A. Lesage, P. Tordo, L. Emsley, J. Am. Chem. Soc. **134** (2012) 2284.

70. B. Kumari, D. John, P. Hoffmann, A. Spende, M. E. Toimil-Molares, C. Trautmann, C. Hess, P. Ruff, R. Stark, M. Schulze, G. Buntkowsky, A. Andrieu-Brunsen, T. Gutmann, Z. für Phys. Chem. (2018) this issue.
71. M. Brodrecht, E. Klotz, C. Lederle, H. Breitzke, B. Stühn, M. Vogel, G. Buntkowsky, Z. für Phys. Chem. (2018) this issue.
72. J. A. Lee, H. Rösner, J. F. Corrigan, Y. Huang, J. Phys. Chem. C **115** (2011) 4738.
73. B. Grünberg, A. Grünberg, H.-H. Limbach, G. Buntkowsky, App. Magn. Res. **44** (2013) 189.
74. E. Roessler, M.Taupitz, K. Börner, M. Schulz, H. M. Vieth, J. Chem. Phys. **92** (1990) 5847.
75. M. Ebener, G. Vonfircks, H. Günther, Helv. Chim. Acta **74** (1991) 1296.
76. M. Ebener, V. Francke, H. Günther, Fresenius J. Anal Chem. **357** (1997) 505.
77. G. von Fircks, H. Hausmann, V. Francke, H. Günther, J. Org. Chem. **62** (1997) 5074.
78. H. Günther, S. Oepen, M. Ebener, V. Francke, Magn. Reson. Chem. **37** (1999) 142.
79. M. F. Harrach, B. Drossel, W. Winschel, T. Gutmann, G. Buntkowsky, J. Phys. Chem. C **119** (2015) 28961.
80. B. J. van Rossum, H. Förster, H. J. M. de Groot, J. Magn. Reson. **124** (1997) 516.